Monthly Notices
of the
ROYAL ASTRONOMICAL SOCIETY

MNRAS **488,** 5042–5047 (2019) doi:10.1093/mnras/stz2041

Energy of a quantum Coulomb liquid

D. A. Baiko★

Ioffe Institute, Politekhnicheskaya 26, 194021 Saint Petersburg, Russian Federation

Accepted 2019 July 8. Received 2019 July 3; in original form 2019 June 6

ABSTRACT

Using the Metropolis method to compute path integrals, the energy of a quantum strongly coupled Coulomb liquid ($1 \leq \Gamma \leq 175$), composed of distinguishable atomic nuclei and a uniform incompressible electron background, is calculated from first principles. The range of temperatures and densities considered represents fully ionized layers of white dwarfs and neutron stars. In particular, the results allow one to determine reliably the heat capacity of ions in dense fluid stellar matter, which is a crucial ingredient for modelling the thermal evolution of compact degenerate stars.

Key words: dense matter – stars: neutron – white dwarfs.

1 INTRODUCTION

A one-component plasma (OCP) is a system of identical point charges immersed into a uniform incompressible background of opposite charge to ensure overall charge neutrality. This system is of paramount importance for the astrophysics of degenerate stars, i.e. white dwarfs and neutron stars, where the point charges are bare atomic nuclei (ions), while a degenerate nearly ideal electron gas constitutes the background. For both types of star, mass densities at which matter can be viewed as an OCP cannot be too low, to ensure that atoms are fully ionized and electron screening is, to a good approximation, negligible. In white dwarfs, the OCP phase may extend all the way down to the centre of the star (i.e. up to the highest available densities); however, several different types of atomic nuclei may be present at some densities simultaneously (e.g. C and O). Studying such a multi-component plasma is beyond the scope of the present article. In neutron stars, matter can be treated as an OCP at least in the outer crust, i.e. all the way up to the neutron-drip density, $\rho_{\rm d} \approx 4.3 \times 10^{11}$ g cm^{-3} (with the same caveat regarding multi-ionic mixtures). It is possible that the same treatment remains valid up to higher, subnuclear, densities (in the inner crust), if the effect of dripped neutrons on the interionic interaction is negligible.

The thermodynamic state of the OCP is described by just two dimensionless parameters. The Coulomb-coupling parameter $\Gamma = Z_i^2 e^2/(aT)$ measures the strength of the typical potential energy with respect to the typical kinetic energy of ions. In this case, T is the temperature ($k_{\rm B} \equiv 1$), Z_i is the ion charge number, e is the elementary charge, and $a = (4\pi n/3)^{-1/3}$ is the ion-sphere radius (n is the ion number density). If one neglects the quantum aspect of the ion motion, Γ alone determines the thermodynamics of the OCP fully. In particular, $\Gamma = 1$ signals the gas–liquid transition, while $\Gamma = \Gamma_{\rm m} \approx 175$ corresponds to the liquid–solid transition. The strength of ionic quantum effects is measured by the second parameter, which can be chosen as the ratio of T to the ion plasma temperature $T_{\rm p} = \hbar\sqrt{4\pi n Z_i^2 e^2/M_i}$, where M_i is the ion mass. In a quantum system, one has $T \ll T_{\rm p}$. Another parameter often used is the ratio $r_{\rm s} = a/a_0$, where $a_0 = \hbar^2/(M_i Z_i^2 e^2)$ is the ionic Bohr radius. These quantities are related to each other as

$$\frac{T}{T_{\rm p}} = \frac{1}{\Gamma}\sqrt{\frac{r_{\rm s}}{3}}\,. \tag{1}$$

The thermodynamics of the OCP has been studied by many authors. In particular, the classic OCP has been studied since the 1960s (Brush, Sahlin & Teller 1966) by Monte Carlo (MC) and molecular dynamics (MD) methods and its thermodynamic properties are now firmly established (e.g. Slattery, Doolen & DeWitt 1982; DeWitt & Slattery 1999; Caillol 1999). The importance of ionic quantum effects in white dwarfs (for cooling, in particular) has been appreciated since about the same time (e.g. Van Horn 1979) and was emphasized once again by Chabrier, Ashcroft & DeWitt (1992). However, there was no practical way to incorporate them. Lamb & Van Horn (1975) have constructed the first quantitative evolutionary model of white dwarfs with realistic thermodynamics, but the treatment of quantum effects was incomplete.

An important study of the quantum OCP from first principles has been conducted by Jones & Ceperley (1996). These authors used the path-integral Monte Carlo method (PIMC), with 54 distinguishable particles in a simulation cell with periodic boundary conditions. For the liquid phase, they have calculated the thermal energy at $\Gamma \leq 160$ and $r_{\rm s} = 100$, 200 and 1200. For carbon, these $r_{\rm s}$ correspond to mass densities $\rho \approx 1.6 \times 10^{13}$, 2×10^{12} and 10^{10} g cm^{-3}, respectively. At such densities, carbon can barely exist, because it burns in nuclear reactions and suffers beta captures. Hence, in practice, the important range for carbon seems to be $r_{\rm s} \gtrsim 1200$. For heavier elements, the situation is similar. For helium, it is possible to attain lower values of $r_{\rm s}$. For instance, according to table 2 of Piersanti, Tornambe &

★ E-mail: baiko@astro.ioffe.ru

Yungelson (2014), helium may be found at $\rho \sim 10^8$ g cm^{-3} ($r_s \approx 140$) and $\Gamma \sim 1$, which, however, is not a very quantum state according to our equation (1). Alternatively, in table 3 of the same work, helium exists at $\rho \sim 10^6$ g cm^{-3} ($r_s \approx 650$) and $\Gamma \sim 50$, which is considerably more quantum.

In the present article, we have decided to focus on the thermodynamics of the strongly coupled liquid regime in the range of densities $r_s \geq 600$, where reliable quantum results are largely absent. The case of higher densities at $\Gamma \sim 1$ is essentially classic (but may be worth a separate study).

2 PATH INTEGRAL MONTE CARLO

Presently, only numerical techniques exist for first-principle studies of quantum strongly coupled Coulomb plasma. This is true for both liquid and solid phases in which all anharmonic effects cannot be accounted for analytically. Following Jones & Ceperley (1996), we employ the PIMC method. Its detailed exposition is given in an extremely helpful review by Ceperley (1995).

In our simulation, there are $N = 250$ distinguishable particles (ions) placed in a cubic simulation cell with periodic boundary conditions. Each particle interacts with all periodic images of the other particles and with the uniform background. Hence, any two particles interact not via the Coulomb potential, but via the Ewald potential, which is the sum of the Coulomb potentials of all periodic images and the background term. In this way, an approximate description of an infinite system is achieved.

In order to calculate various thermodynamic averages for a quantum system, it is represented by a classic one, in which N quantum particles are replaced by N classic ring polymers with M numbered nodes ('beads') each and M links connecting beads with consecutive numbers (M is a positive integer). In each ring, there is an interaction between any two linked beads, which does not allow them to move arbitrarily far away from each other ('kinetic spring'). There is also an effective interaction between polymers originating from an interaction between beads having the same number in all rings.

If the effective interaction (known as 'link action': see Ceperley 1995, for details) were known exactly, then the classic and quantum systems would be exactly isomorphic for any M. However, this is not the case, and various approximations for the link action have been proposed. The simplest of them is known as the *primitive* approximation. Within its framework, the link action is directly related to the actual potential energy of N beads having the same number in their respective rings and interacting only between themselves via the Ewald potential. The primitive approximation can be shown to become exact in the $M \to \infty$ limit.

Ceperley (1995) emphasized the utility of another approximation, *pair action*, for its ability to produce correct results at smaller M than the primitive approximation in some problems (see also Militzer & Graham 2006; Militzer 2016). A smaller M translates into less time-consuming computations. We have managed to construct the pair action for the Ewald potential including off-diagonal terms for practically relevant ranges of action arguments (not too close to zero and not too far off the diagonal). However, it has been found that the primitive approximation reproduced the zero-point energy of a Coulomb crystal (the major contribution to which is given by the well-known harmonic lattice value) at smaller M than the pair action. Consequently, we have chosen to use the primitive approximation for the action in this study.

In the primitive approximation, one needs to sample the probability distribution

$$\pi(R_1, R_2, \ldots, R_M = R_0) = \frac{1}{Z} \exp\left[-\sum_{m=1}^{M} S_m\right],$$
$$e^{-S_m} = \frac{1}{(4\pi\lambda\tau)^{3N/2}} \exp\left\{-\left[\frac{(R_m - R_{m-1})^2}{4\lambda\tau} + \tau V(R_m)\right]\right\}, \quad (2)$$

where R_m denotes the three Cartesian coordinates of all N beads with number m, i.e. 750 numbers in our simulation (beads 0 are the same as beads M). Furthermore, Z is the partition function, which ensures that the distribution π is normalized, $\lambda = \hbar^2/(2M_i)$, $\tau = 1/(MT)$, and $V(R_m)$ is the potential energy of all beads of number m.

The sampling was done with the aid of the Metropolis algorithm. We have combined two types of move: a single bead moves using free-particle sampling and 'classic' moves. In the latter, we attempted to move a polymer as a whole using uniform sampling probability density within a cube with size chosen to ensure decent move acceptance rates. The latter type of move has improved the quality of our results considerably at nearly classic ρ and T.

The following quantity was used as the energy estimator (thermodynamic estimator):

$$E = \left\langle \frac{3N}{2\tau} - \frac{(R_m - R_{m-1})^2}{4\lambda\tau^2} + V(R_m) \right\rangle, \quad (3)$$

where m is an arbitrary integer between 1 and M, to which the results should not be sensitive. Angle brackets mean averaging with the probability distribution (2).

3 RESULTS

The thermal energy of the liquid (equal to the total internal energy minus the Madelung energy of the body-centred cubic lattice, E_0) calculated by the method described in Section 2 is presented in Fig. 1(a) and Table 1. Dots in Fig. 1(a) are computational results (including the extrapolation procedure below), while solid lines simply connect them to improve graph readability. We have calculated the thermal energy for 25 values of Γ evenly spaced between 1 and 175 ($\Delta\Gamma = 7.25$) and for 15 values of $r_s = 600$, 750, 950, 1200, 1500, 1900, 2400, 3000, 3800, 4800, 6000, 8600, 15 000, 30 000 and 120 000. This corresponds to ~7 orders of density variation and, e.g. for carbon, spans the range from 10^4–8×10^{10} g cm^{-3}, while for helium the respective range of densities is from 0.2–10^6 g cm^{-3}. Calculations are unreliable at the lower end of the density range and those Z_i for which complete ionization is not reached, because electronic degrees of freedom are not taken into account. Solid curves with dots correspond to different r_s, with the $r_s = 600$ curve being on top, $r_s = 750$ the second curve from the top, $r_s = 950$ the third, etc., and, finally, $r_s = 120\,000$ is the second curve from the bottom. The (red in the online version) curve at the very bottom shows the classic liquid thermal energy as calculated by Caillol (1999) and fitted by Potekhin & Chabrier (2000).

In Fig. 1(b), we compare solid curves from Fig. 1(a) for $r_s = 600$, 1500, 2400, 4800, 8600 and 15 000 with the thermal energy of the classic liquid combined with the first quantum Wigner–Kirkwood correction (Hansen 1973) at the same r_s (dotted curves). Long dashes also include the second quantum correction of Hansen & Viellefosse (1975). The agreement with our results is quite good in the more classic range of parameters, but becomes worse with decreasing r_s or decreasing T (i.e. increasing Γ). The first quantum correction provides an adequate description of our computed values for all Γ in the liquid at $r_s \gtrsim 20\,000$. The Hansen–Viellefosse term

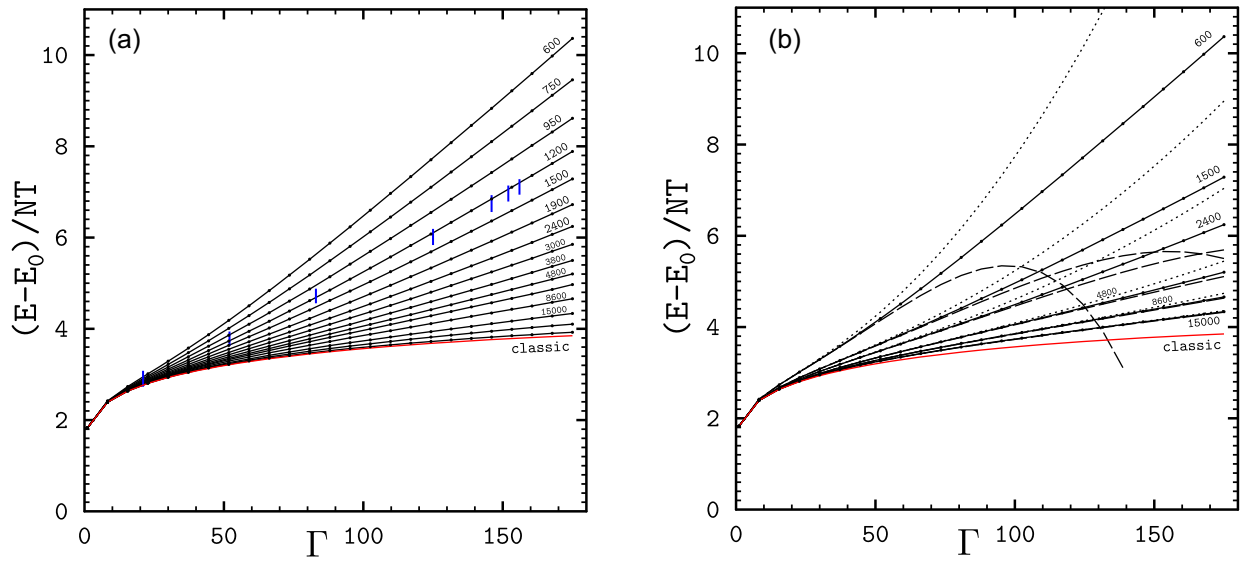

Figure 1. (a) Calculated thermal energy of a Coulomb liquid versus Γ. From top to bottom: $r_s = 600$, 750, 950, 1200, 1500, 1900, 2400, 3000, 3800, 4800, 6000, 8600, 15 000, 30 000 and 120 000. The curve at the very bottom (red in the online version) is the classic liquid energy. Bars represent selected data points of Jones & Ceperley (1996) at $r_s = 1200$. (b) Same as in panel (a) but for $r_s = 600$, 1500, 2400, 4800, 8600 and 15 000 only. Dotted and long-dashed curves incorporate, respectively, the first and the second quantum Wigner–Kirkwood corrections to the classic energy.

Table 1. Numerical results for $(E - E_0)/NT$.

	r_s														
Γ	600	750	950	1200	1500	1900	2400	3000	3800	4800	6000	8600	15e3	3e4	12e4
175.00	10.364	9.457	8.613	7.886	7.285	6.723	6.244	5.851	5.499	5.202	4.970	4.659	4.336	4.102	3.924
167.75	9.979	9.118	8.313	7.624	7.050	6.519	6.070	5.700	5.367	5.086	4.862	4.581	4.281	4.067	3.901
160.50	9.595	8.778	8.020	7.362	6.820	6.320	5.893	5.544	5.234	4.975	4.763	4.500	4.226	4.028	3.871
153.25	9.216	8.440	7.723	7.103	6.591	6.120	5.719	5.396	5.101	4.860	4.665	4.430	4.169	3.989	3.850
146.00	8.832	8.103	7.426	6.846	6.363	5.920	5.546	5.247	4.973	4.753	4.570	4.346	4.115	3.946	3.818
138.75	8.457	7.771	7.131	6.588	6.138	5.723	5.379	5.095	4.844	4.640	4.480	4.273	4.052	3.908	3.788
131.50	8.080	7.436	6.838	6.332	5.913	5.530	5.210	4.948	4.718	4.526	4.379	4.193	3.997	3.861	3.756
124.25	7.705	7.103	6.549	6.077	5.686	5.332	5.038	4.804	4.594	4.418	4.286	4.113	3.937	3.820	3.723
117.00	7.335	6.775	6.267	5.826	5.468	5.143	4.873	4.655	4.468	4.310	4.188	4.038	3.882	3.769	3.685
109.75	6.968	6.449	5.977	5.575	5.252	4.954	4.712	4.513	4.343	4.205	4.098	3.958	3.821	3.723	3.648
102.50	6.599	6.127	5.698	5.331	5.035	4.767	4.546	4.371	4.221	4.097	3.998	3.880	3.756	3.672	3.608
95.25	6.235	5.807	5.418	5.088	4.827	4.584	4.388	4.236	4.096	3.992	3.904	3.804	3.696	3.622	3.568
88.00	5.878	5.492	5.141	4.848	4.623	4.405	4.232	4.098	3.979	3.885	3.812	3.721	3.633	3.568	3.521
80.75	5.526	5.184	4.872	4.618	4.411	4.224	4.083	3.963	3.862	3.779	3.717	3.643	3.562	3.510	3.470
73.50	5.176	4.876	4.607	4.389	4.215	4.053	3.930	3.830	3.740	3.675	3.622	3.556	3.494	3.448	3.416
66.25	4.837	4.578	4.352	4.165	4.018	3.885	3.779	3.698	3.624	3.569	3.526	3.471	3.419	3.384	3.357
59.00	4.504	4.289	4.100	3.944	3.825	3.716	3.626	3.563	3.507	3.460	3.428	3.387	3.340	3.313	3.296
51.75	4.186	4.010	3.859	3.731	3.636	3.551	3.479	3.427	3.384	3.351	3.325	3.290	3.257	3.236	3.220
44.50	3.871	3.735	3.619	3.524	3.450	3.386	3.334	3.296	3.263	3.234	3.215	3.190	3.168	3.152	3.141
37.25	3.578	3.477	3.387	3.321	3.267	3.221	3.186	3.159	3.132	3.114	3.100	3.084	3.065	3.054	3.048
30.00	3.290	3.225	3.167	3.117	3.083	3.051	3.029	3.009	2.995	2.982	2.973	2.962	2.951	2.942	2.937
22.75	3.014	2.969	2.940	2.911	2.892	2.873	2.858	2.847	2.839	2.832	2.828	2.820	2.814	2.809	2.808
15.50	2.735	2.715	2.697	2.686	2.677	2.668	2.660	2.657	2.652	2.648	2.645	2.644	2.640	2.638	2.636
8.25	2.418	2.414	2.408	2.405	2.404	2.401	2.397	2.395	2.395	2.396	2.393	2.394	2.392	2.391	2.392
1.00	1.825	1.825	1.825	1.825	1.826	1.826	1.825	1.825	1.825	1.825	1.826	1.826	1.825	1.825	1.825

extends this range down to $r_s \gtrsim 10\,000$. [For $r_s = 1200$, these approximations are also plotted in Fig. 2(a).]

There are three sorts of errors that need to be addressed. First, there is a statistical error stemming from the limited number of steps in the Metropolis algorithm. This error manifests itself as a dependence of energies on initial conditions, random seeds or the number m in equation (3). We have analysed these dependences for a few combinations of r_s and T and concluded that the confidence interval could be estimated at the 90 per cent level as ±0.007 (in absolute units) for the entire dataset. This is smaller than the dot sizes in Fig. 1(a). A much more extended computation is needed for a rigorous statistical evaluation of our data.

Secondly, there is a systematic error associated with the finite polymer size M. In order to reduce this error, we have performed PIMC calculations with four values of M: $M_{\rm min}$, $2M_{\rm min}$, $4M_{\rm min}$ and $M_{\rm max} = 8M_{\rm min}$. For illustration, the respective energies at $r_s = 1200$

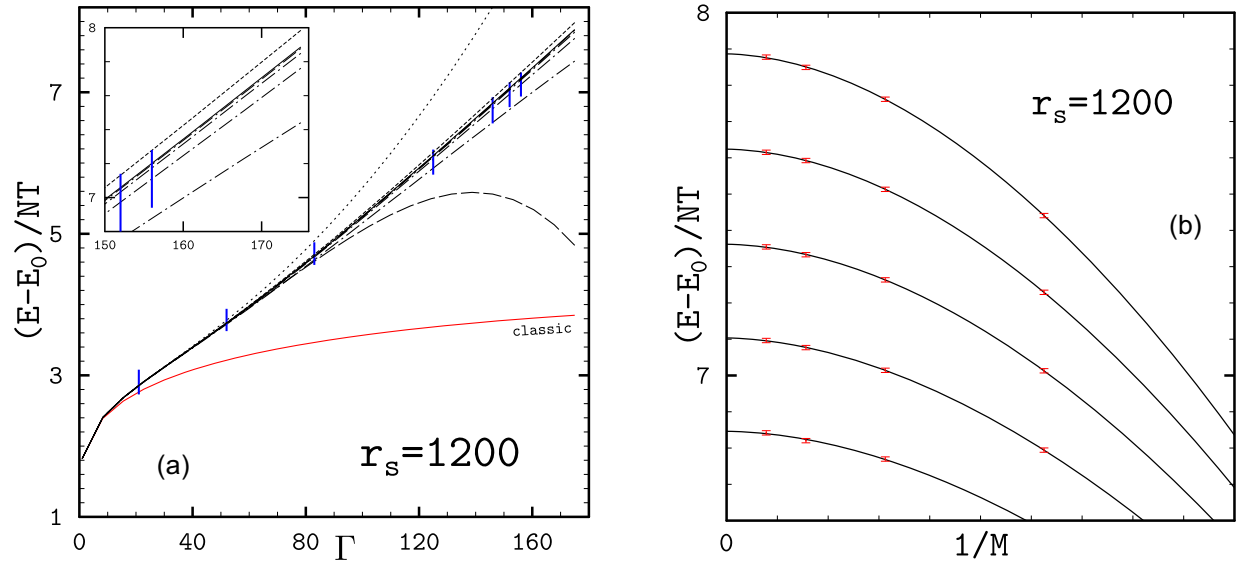

Figure 2. (a) Various results at $r_s = 1200$. Four dot–dashed curves are calculations at different M (higher curves correspond to larger M). The solid curve (nearly merging with the top dot–dashed curve) shows the data extrapolated to $1/M = 0$. The short-dashed curve includes a finite N correction, equation (4). Dotted and long-dashed lines display the same Wigner–Kirkwood approximations as in Fig. 1(b). Bars represent selected data points of Jones & Ceperley (1996). (b) Extrapolation of calculated energies from finite M to $1/M = 0$ at $r_s = 1200$ and the five largest values of Γ.

are plotted in Fig. 2(a) by dot–dashed curves: M_{max} is the top one and all the others become progressively lower with decreasing M. At each r_s and Γ, these data have been extrapolated as functions of $1/M$ down to $1/M = 0$. An example of this procedure is given in Fig. 2(b) for $r_s = 1200$ and several values of Γ. The resulting dependence represents the exact quantum energy of 250 distinguishable particles under periodic boundary conditions. For $r_s = 1200$, it is plotted in Fig. 2(a) by the solid line, nearly merging with the top dot–dashed line. It is these extrapolated data that are presented in Fig. 1(a) and Table 1.

Bars in Figs 1(a) and 2(a) represent the actual height and position of triangles from the bottom panel of fig. 3 of Jones & Ceperley (1996). We see, that at $r_s = 1200$, our results are compatible with theirs.

Thirdly, there is a systematic error due to the finite number of particles in our simulation, $N = 250$. In principle, a conclusive study of N dependence must include similar calculations at several different N, which is time-consuming; we defer it to a future work (see also Holzmann et al. 2016). Based on studies of smaller systems, Jones & Ceperley (1996) had come up with the following formula (their equation 2):

$$\frac{\mathcal{E}_N - \mathcal{E}_\infty}{T} = [0.035(18) - 0.0018(1)\Gamma]\,\frac{\Gamma}{2N}, \qquad (4)$$

where $\mathcal{E}_N$ and $\mathcal{E}_\infty$ are per-particle energies in the finite system and the thermodynamic limit, respectively, and we have taken into account that their energies were expressed in ionic Rydbergs. This correction applied to $r_s = 1200$ produces, as the $N \to \infty$ limit, the short-dashed curve in Fig. 2(a), which barely touches the bars. Remarkably, the correction does not depend on r_s (cf. the right-hand side of equation 4) and thus it will be of about the same absolute magnitude at higher r_s. However, this can hardly be the case, because at high r_s our numerical data are in much better agreement with the classic results plus quantum corrections, which implies that, at these r_s, N correction must be negligible. In view of this controversy, we have chosen not to apply the finite N correction of Jones & Ceperley (1996) in the present work, pending a detailed future study.

4 DISCUSSION AND OUTLOOK

Our results can be used to derive the thermodynamic properties of matter necessary for modelling various physical phenomena in compact stellar objects.

First of all, the change in ion energy due to quantum effects studied in the present article produces a change of the ion pressure and thus a slight modification of the equation of state in white dwarf cores and neutron star crusts. This effect is expected to be small, though, because the total pressure is dominated by degenerate electrons.

The thermal properties of matter are modified in a more meaningful way. Consider, for instance, heat capacity. Over a wide range of parameters, the heat capacity is dominated by ions. This quantity is very important for a number of astrophysical applications. For one, it determines cooling of white dwarfs. Reliable modelling of this process allows one to interpret the observed white dwarf luminosity function and extract a fundamental parameter such as the age of the local Galactic disc (e.g. D'Antona & Mazzitelli 1990). The heat capacity of a Coulomb liquid is also needed to understand the observed real-time cooling of neutron star crusts heated during episodes of accretion in X-ray transients (e.g. Deibel et al. 2017), although in this case temperatures may be too high for quantum effects to be noticeable. Another promising research route is the thermal evolution of accreting white dwarfs in cataclysmic variables (e.g. Gänsicke 2000).

Let us analyse two representative examples: carbon at $\rho \approx 3 \times 10^8$ g cm^{-3} ($r_s = 3800$) and helium at $\rho \approx 6.6 \times 10^5$ g cm^{-3} ($r_s = 750$). The ion specific heat at constant volume is

$$\frac{C}{N} = \frac{1}{N}\left(\frac{\partial E}{\partial T}\right)_V, \qquad (5)$$

where E is the energy calculated in the previous section. The specific heat of carbon and helium is plotted in Fig. 3(a) and (b) as a function of temperature across the melting transition. For the sake of this illustration, we have assumed that melting takes place at $\Gamma_m = 175$. We are aware of the fact that Γ_m is a weak function

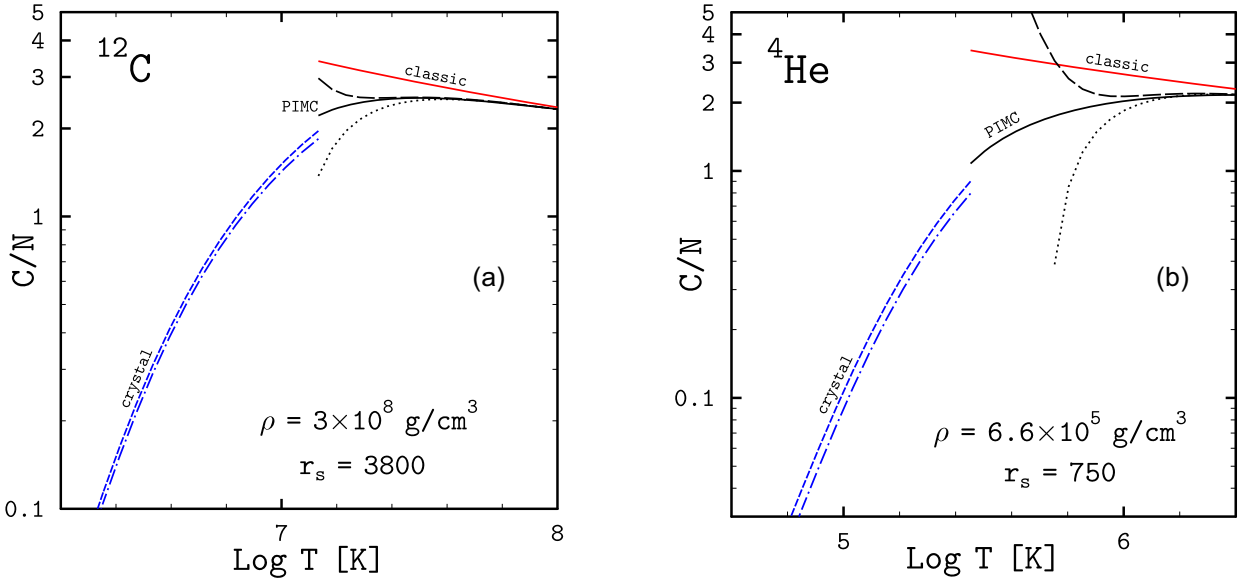

Figure 3. (a) Ion specific heat of carbon at $\rho \approx 3 \times 10^8$ g cm^{-3}. Shown are PIMC results in the liquid phase (solid curve), specific heat of the classic liquid (upper solid curve, red in the online version), first quantum correction in the liquid (dots), second quantum correction in the liquid (long dashes), harmonic lattice results in the crystal phase (dot–dashed curve, blue in the online version) and quantum anharmonic correction in the crystal (short dashes, blue in the online version). (b) Same as in panel (a), but for helium at $\rho \approx 6.6 \times 10^5$ g cm^{-3}.

of r_s due to quantum effects, but an accurate determination of this function requires extra work and is beyond the scope of the present article. At lower temperatures (T to the left of the discontinuities), a body-centred cubic crystal phase takes place, the specific heat of which is known very accurately in the harmonic approximation (Baiko, Potekhin & Yakovlev 2001). It is shown by the (blue in the online version) dot–dashed curve. The (blue in the online version) short-dashed curve includes a quantum anharmonic contribution calculated in a model-dependent way by Chugunov & Baiko (2005).

In the liquid phase, we plot the various approximations mentioned in Section 3. The upper solid curve (red in the online version) shows the specific heat of the classic liquid OCP derived from fits of Potekhin & Chabrier (2000). Dots include the first quantum correction to the classic values obtained from the Wigner–Kirkwood (WK) expansion (Hansen 1973). The long-dashed curve includes the second WK correction derived by Hansen & Viellefosse (1975). Our PIMC results are shown by the solid curve. In order to plot it, we have fitted our energy data at fixed r_s by a smooth curve and differentiated it with respect to T.

It is interesting to observe that the specific heat jump at melting (at quantum temperatures) appears to be much smaller with quantum effects included from first principles than with various approximations available previously. A more complete assessment of this result will be made when first-principle thermodynamics of the solid phase becomes available. More importantly, from a practical point of view, our data indicate that the classic approximation for the specific heat can seriously overestimate it, while addition of the first WK correction yields an equally serious underestimation. The total heat capacity of a star, which determines its cooling rate, is an integral of the specific heat over the star. The degree to which the total heat capacity is affected by quantum phenomena thus depends on the central density, temperature and composition. A preliminary estimate suggests that in certain situations the actual heat capacity of a star may be as low as two-thirds of the respective classic value.

Besides carbon and helium, it is just as easy to consider heavier elements. However, in order to produce quantum effects of comparable size, one would have to go to much higher densities. Since r_s scales as $\rho^{-1/3} Z_i^2 M_i^{4/3}$, to achieve $r_s = 3800$, one would require $\rho = 5.3 \times 10^9$ g cm^{-3} for ^{16}O and $\rho = 9.4 \times 10^{14}$ g cm^{-3} for ^{56}Fe (the latter is impossible, because such a ρ exceeds the nuclear saturation density). In the standard picture, with growth of the mass density, lighter elements burn into heavier ones in nuclear reactions. The maximum density for a given light element to exist at a given temperature is a function of the nuclear reaction rates in a strongly coupled plasma. It is clear from the present study that these reactions occur in the regime where quantum effects are well pronounced. Their rates are thus determined by the underlying quantum dynamics of ions and are extremely sensitive to small variations of density and temperature (e.g. Pollock & Militzer 2004). Accordingly, it seems worthwhile to analyse the rates in detail from first principles, which would require a minor modification of our code. Such a study would have implications for a wide range of astrophysical phenomena, from bursts and flashes in compact stars to SN Ia.

Another thermal property that is expected to be sensitive to quantum effects is $\chi_T = (\mathrm{d}\ln P/\mathrm{d}\ln T)_V$, where P is the total pressure. This parameter is similar to the specific heat, equation (5). In both cases, one needs to differentiate a quantity dominated by degenerate electrons (energy in the case of C and pressure in the case of χ_T). However, the differentiation is with respect to temperature, which means that only the thermal components of E and P really matter. This leads to a domination of ion contributions over those due to degenerate electrons. Compressibility χ_T sets the scale of the Brunt–Väisälä frequency (e.g. Brassard et al. 1991), which, in turn, determines the main properties of stellar g modes (e.g. Montgomery & Winget 1999). Quantum effects may change the profile of the Brunt–Väisälä frequency over a large fraction of the stellar radius. This may result in an observable change of the predicted seismological data for white dwarfs.

The present work can be also extended in other directions. An accurate energy of the solid phase can be calculated, which, among other things, would allow one to determine the dependence of the

latent heat of crystallization on r_s due to quantum effects. Latent heat of crystallization is another crucial parameter in the theory of white dwarf cooling. Its release delays cooling and directly affects the estimated age of the stellar population. A preliminary analysis (assuming fixed $\Gamma_m = 175$) indicates that the latent heat is a weak function of r_s, decreasing from $\approx 0.77\,T$ in the classic limit to $\approx 0.71\,T$ at $r_s = 1200$. A small correction to this dependence due to the r_s dependence of Γ_m is expected. Similar studies of multi-ionic mixtures can be performed with minor modifications of the same code. Finally, weak electron screening of the ion potential can be included, but this will introduce an extra physical parameter into the problem.

ACKNOWLEDGEMENTS

The author is sincerely grateful to A. A. Danilenko and D. G. Yakovlev for help and discussions. This work was supported by the Russian Science Foundation grant 19-12-00133.

REFERENCES

Baiko D. A., Potekhin A. Y., Yakovlev D. G., 2001, Phys. Rev. E, 64, 057402
Brassard P., Fontaine G., Wesemael F., Kawaler S. D., Tassoul M., 1991, ApJ, 367, 601
Brush S. G., Sahlin H. L., Teller E., 1966, J. Chem. Phys., 45, 2102
Caillol J. M., 1999, J. Chem. Phys., 111, 6538
Ceperley D. M., 1995, Rev. Mod. Phys., 67, 279
Chabrier G., Ashcroft N. W., DeWitt H. E., 1992, Nature, 360, 48
Chugunov A. I., Baiko D. A., 2005, Physica A, 352, 397
D'Antona F., Mazzitelli I., 1990, ARA&A, 28, 139
Deibel A., Cumming A., Brown E. F., Reddy S., 2017, ApJ, 839, 95
DeWitt H. E., Slattery W. L., 1999, Contrib. Plasm. Phys., 39, 97
Gänsicke B. T., 2000, Rev. Mod. Astron., 13, 151
Hansen J. P., 1973, Phys. Rev. A, 8, 3096
Hansen J. P., Viellefosse P., 1975, Phys. Lett. A, 53, 187
Holzmann M., Clay R. C., III, Morales M. A., Tubman N. M., Ceperley D. M., Pierleoni C., 2016, Phys. Rev. B, 94, 035126
Jones M. D., Ceperley D. M., 1996, Phys. Rev. Lett., 76, 4572
Lamb D. Q., Van Horn H. M., 1975, ApJ, 200, 306
Militzer B., 2016, Comp. Phys. Comm., 204, 88
Militzer B., Graham R. L., 2006, J. Phys. Chem. Sol., 67, 2136
Montgomery M. H., Winget D. E., 1999, ApJ, 526, 976
Piersanti L., Tornambe A., Yungelson L. R., 2014, MNRAS, 445, 3239
Pollock E. L., Militzer B., 2004, Phys. Rev. Lett., 92, 021101
Potekhin A. Y., Chabrier G., 2000, Phys. Rev. E, 62, 8554
Slattery W. L., Doolen G. D., DeWitt H. E., 1982, Phys. Rev. A, 26, 2255
Van Horn H. M., 1979, Physics Today, Jan., 23

This paper has been typeset from a TEX/LATEX file prepared by the author.